C. R. Chimie 21 (2018) 310–317

Contents lists available at ScienceDirect

Comptes Rendus Chimie

www.sciencedirect.com

Full paper/Mémoire

Plasma generation in liquid as a new efficient synthesis approach of titania–zinc ferrite nano(photo)catalyst

Maria Ignat [a, b, **], Petrisor Samoila [b, *], Cristina Coromelci [a], Liviu Sacarescu [b], Iulian Asaftei [a], Valeria Harabagiu [b], Camelia Miron [c]

[a] Alexandru Ioan Cuza University, Department of Chemistry, 11, Carol I Boulevard, 700506, Iasi, Romania
[b] Petru Poni Institute of Macromolecular Chemistry, Aleea Grigore Ghica Voda 41 A, 700487, Iasi, Romania
[c] Leibniz-Institute for Plasma Science & Technology, 17489, Greifswald, Germany

ARTICLE INFO

Article history:
Received 31 January 2017
Accepted 22 May 2017
Available online 19 June 2017

Keywords:
Titania–zinc ferrite nanocomposites
Liquid phase plasma
Reaction time
Visible light photocatalyst
Rhodamine 6G

ABSTRACT

In the past years, an important problem that requires solutions at the global scale is the environmental pollution. This work describes a possible approach toward finding such solutions based on nanophotocatalysts with improved activity. Thus, the present study reports a new and efficient synthesis procedure for titania–zinc ferrite nanocomposite with enhanced photodegradation activity. The method is based on the liquid phase plasma technique and follows a bottom-up scheme. The resulted materials have been compared with those synthesized by the ultrasound-assisted method. Using the plasma-assisted procedures in the fabrication of an efficient nano(photo)catalyst decreases considerably the reaction time. The liquid phase plasma generates nanoparticles with enhanced structural, textural, and morphological properties as demonstrated by X-ray diffraction, nitrogen sorption, transmission electron microscopy, and small-angle X-ray scattering.

1. Introduction

The environmental pollution represents one of the greatest problems and a major threat at the global scale. This is the reason why, during the past decades, an appreciable number of researches focused their efforts on finding new photocatalytic solutions [1]. As well known, most of the existing photocatalysts used in the decomposition of organic pollutants are efficient under ultraviolet (UV) irradiation only. Therefore, there is an increasing demand for visible light–activated photocatalysts with a smaller band gap [2,3]. In this respect, a promising approach is to use zinc ferrite (ZF) nanoparticles as a doping agent for narrowing the band gap of the classical titania photocatalyst [2,4]. This idea is advantageous because the ZF can be prepared relatively easily, with low costs, and has a band gap value in the range of 1.0 and 2.0 eV (depending on its chemical composition and synthesis method), being chemically and physically stable in the photodegradation medium [1,5–8].

Generally, the synthesis of titania–ZF nanocomposites may be achieved by one-pot synthetic methods (coprecipitation) [7] or by two-step methods [8,9]. The later has two possible preparation routes. The first one considers the preparation of the spinel ferrite in the presence of a preobtained mesoporous titania [8], whereas the second one proposes the synthesis of titanium dioxide in the presence of the presynthesized ZF nanoparticles [9]. Our

* Corresponding author.
** Corresponding author. Alexandru Ioan Cuza University, Department of Chemistry, 11, Carol I Boulevard, 700506 Iasi, Romania.
E-mail addresses: ignat.maria@icmpp.ro (M. Ignat), samoila.petrisor@icmpp.ro (P. Samoila).

http://dx.doi.org/10.1016/j.crci.2017.05.006
1631-0748/

previous study reports the importance of the addition order of components used in the synthesis and its influence over the properties of the titania–ZF nanocomposite [10]. In that case, the synthesis procedure has been assisted by ultrasonication (US). Thus, the resulted mesoporous titania prepared in the presence of ZF nanoparticles lead to a nanocomposite with improved photocatalytic activity. Furthermore, our interest was to find another technique for the synthesis of titania in the presence of presynthesized ZF nanoparticles to increase the efficiency of the titania–ZF nanophotocatalyst. Plasma generation in liquid [11] at atmospheric pressure has been used in thin film deposition, but its application in nanofabrication following the bottom-up scheme is quite new [12]. The generation of pulse electrical discharge in liquids for material modification is a novel approach that has a high potential because of the high flexibility related to possible applications. Different processes in plasma generated in liquids produce reactions determined by the way the electrical energy is provided and dissipated. Chemically active species, such as ions, radicals, metastable excited atoms, and UV photons are formed in the discharge, leading to a rapid and efficient metal nanoparticle synthesis [13–15].

The present work reports the synthesis of titanium oxide nanoparticles in the presence of ZF nanoparticles by the liquid phase plasma (LPP) reduction process. This method was selected with the purpose to reduce the preparation time and for cost saving at the industrial scale [16]. This technique has been compared with the US method applied for preparation of the titania–ZF nanocomposite having the same composition, as reported in a previous work [10]. It was found that the LPP method is about 10 times faster compared with the previously mentioned US technique. The composite nanomaterials have been prepared in a solution using titania precursor and ZF nanoparticles. To generate the electrical discharge in the aqueous mixture, a bipolar pulsed power supply was used. The porous titanium oxide nanoparticles were formed in the presence of F127 surfactant. A secondary porosity has been observed after a longer time plasma treatment. The final composition of the synthesized nanomaterials was $10ZnFe_2O_4$–$90TiO_2$ (wt %). All the resulted samples have been characterized from structural, textural, and morphological point of view.

This study emphasizes the advantages of using the liquid-phase plasma technique in the synthesis of the titania–ZF nanocomposite compared with US method. The obtained results show that the LPP-assisted synthesis of the visible-active titania–ZF nanophotocatalyst allows shorter reaction time, leading to the formation of nanoparticles with improved properties as proved by the Rhodamine 6G (R6G) photodegradation tests.

2. Experimental section

2.1. Synthesis of ZF nanoparticles

The ZF nanoparticles, with molecular formula $ZnFe_2O_4$, were prepared by the sol–gel autocombustion method as previously described [17].

2.2. Synthesis of porous titanium dioxide in the presence of ZF nanoparticles by US technique

In a typical synthesis, 10% Pluronic F127 in a 1:1 water/isopropanol mixture was prepared under US for 1 h, using a horn-probe sonic tip (VibraCell, 750W) at 25% of amplitude with ON/OFF cycle set for 2 s. When the solution became clear the titanium isopropoxide (TIPO) was added as the titania source (the weight ratio F127/TIPO = 1/1.7). Then, this reaction mixture was subjected to US (1 h). The resulted gel was filtered, washed several times with distilled water, and dried at room temperature. The obtained powder was further calcined at 450 °C to remove F127 surfactant from the system.

2.3. Plasma generation in liquid reaction mixture

Pulsed electrical discharges were generated in a cylindrical Pyrex vessel between tungsten electrodes immersed in the 20 mL nano(photo)catalyst precursor solution. Ceramic tubes were used as an insulator material (Nilaco), and the protrusion of the electrodes from the insulation was 1 mm, with a flat end. The electrodes of 1 mm diameter (99% purity, Nilaco) were placed in the center of the vessel in a rod-to-rod configuration. The interelectrode gap was set to 1 mm. The experimental configuration is presented elsewhere [18,19]. In all the performed experiments the applied pulsed voltage was provided by a unipolar power supply having a 30-μs rise time—5 kV maximum voltage pulse. The voltage pulse width was set to 2 μs and the repetition frequency was 16 kHz. In the cylindrical Pyrex vessel was introduced the reaction mixture obtained as described previously. For the synthesis of **TZF 4pl** sample, the discharge time was set for 4 min, whereas for the synthesis of **TZF 5pl** sample the discharge time was raised up to 5 minutes. The current and voltage waveforms were measured using a current probe (Tektronix P-6021) and a voltage probe (Tektronix P-6015) respectively, connected to an oscilloscope (Tektronix TDS 310). The resulted gels were subjected to the same thermal treatments as described for the US technique.

The resulted nano(photo)catalyst obtained by the ultrasound-assisted method was labeled as **TZF us**, whereas those obtained by plasma treatment were labeled as **TZF pl**. The final compositions of the nano(photo)catalysts were $ZnFe_2O_4$:TiO_2 = 10:90 (wt %).

2.4. Characterization methods and equipment used

A Bruker-AXS D8 Advance powder diffraction system, equipped with a transmission-type goniometer, using Cu Kα radiation (λ = 1.5406 Å) was used for the structural characterization of the synthesized samples. The X-ray diffraction (XRD) patterns were obtained in the range of 10–80 $2\theta^{\circ}$, using a scanning step of 0.02°/s.

Transmission electron microscopy (TEM) was used for the morphological characterization of the samples. The TEM images were obtained on a Hitachi HT7700 microscope equipped with a Bruker XFlash 6 EDS detector operated at 120 kV in high contrast mode. The samples were prepared by dispersing the powders in ethanol using

an ultrasound bath and then placing a small drop of dispersions on the TEM grids. Finally, before the measurements, the solvent was removed by evaporation at 50 °C overnight.

The small-angle X-ray scattering (SAXS) technique was used to determine the particle size distribution and average particle sizes. The data have been acquired on a Bruker-Nanostar U machine equipped with three-pinhole collimation optics. Because of its precisely parallel X-ray beam, with a virtually no background and a high intensity, the measuring time was very short and the resolution was very high. The scattering intensity is plotted as a function of scattering vector $q = (4\pi/\lambda)\sin\theta$, where θ is half the scattering angle and λ is the X-ray wavelength (Cu Kα = 1.54 Å).

The nitrogen sorption isotherms were recorded on a Quantachrome Nova 2200 automated gas adsorption system using nitrogen adsorbate at −196 °C, for the material textural characterization. Before recording sorption isotherms, all samples were outgassed for 2 h at room temperature in high vacuum. Brunauer–Emmet–Teller (BET) equation was used to calculate the specific surface area. The total pore volume was taken directly from the isotherm, at $P/P_0 = 0.95$. The pore size distributions (PSDs) were estimated from the adsorption branch of the nitrogen isotherm using the Barett–Joyner–Halenda equation.

The optical absorption properties of the synthesized samples were investigated with a UV–visible diffuse reflectance (UV–vis DR) spectrophotometer, type Shimadzu UV-2450. The "solid solutions" of the synthesized samples in MgO, as white reference, were prepared and pressed into pellets. The Kubelka–Munk function $(F(R) = (1-R)^2/2R = k/s = Ac/s$, where R is the reflectance, k is the absorption coefficient, s is the scattering coefficient, c is the concentration of the absorbing species, and A is the absorbance, was applied to the recorded spectra to obtain Tauc plots providing information about the band gap energy [20].

2.5. Photocatalytic activity

To study the photocatalytic activity of the nanocomposite samples, the decomposition tests of R6G ($C_{28}H_{31}N_2O_3Cl$) under visible light irradiation were performed. The degradation experiments occurred in a cylindrical photoreactor equipped with a mercury medium pressure lamp (TQ 150 Z1) of 400–450 nm radiation intensity. The lamp was surrounded by a circulating water jacket to avoid the heating of the reaction mixture and to keep the temperature constant. In a typical photocatalytic experiment, 0.1 g of the powdered sample was suspended in a 300 mL R6G solution of 20 mg/L and magnetically stirred during the experiment. The adsorption–desorption equilibrium was reached after 30 min of the photocatalyst –dye solution contact. Then, the lamp was switched on to start the photodegradation process. Several time intervals (0, 5, 10, 15, 20, 30, 45, 60, and 90 min) were selected to investigate and evaluate the changes in the R6G concentration in solution. To evaluate the R6G concentration, a calibration curve was determined using the absorption maximum at 526 nm.

3. Results and discussions

The synthesis procedures used for the titania–ZF nanocomposites, follow the flowchart depicted in Fig. 1. As mentioned, the ZF nanoparticles were synthesized by the sol–gel autocombustion method (described elsewhere [10]) before the synthesis of the titania material. Then, the mesoporous TiO_2 was synthesized in the presence of ZF nanoparticles using two methods: ultrasound-assisted sol –gel method and LPP. The effect of the selected preparation procedures on the textural, structural, and morphological characteristics and photocatalytic activity of the composites were further studied.

3.1. Characterization of the nanocomposites samples

To study and compare the features of the titania–ZF nanocomposites obtained by liquid plasma processing and US several techniques were used as follows.

The nitrogen adsorption–desorption isotherms were recorded for textural parameter determination. The nitrogen sorption isotherms and the corresponding PSDs of all the nanocomposite samples are presented in Fig. 2. According to IUPAC classification, these are categorized as type IV isotherms, specific to mesoporous adsorbents [8,12,15,18]. In all cases, the pore filling process with nitrogen molecules is given by the condensation process of the nitrogen gas to liquid-like phase. Thus, the capillary condensation step occurs at different relative pressures, varying from one sample to another, and its steepness (Fig. 2). Also, the capillary condensation that is accompanied by the hysteresis should be noted. Its presence indicates that our materials have cylindrical mesopores wider than ~4 nm [21]. Hence, the isotherm for the **TZF us** sample shows a composite hysteresis loop, of types I and II, where the more pronounced uptake (filling of micropores) occurs at low relative pressures. Such a combined hysteresis loop is of type H4, which is typical for micro-mesoporous materials with slit-like pores [20]. On the other hand, the isotherms for the **TZF pl** samples exhibit a hysteresis close to the type H1, which is characteristic to porous materials with a narrow range of uniform mesopores [22]. This assumption is sustained by the (drawn) PSDs, which is more visible on the PSD curve calculated from the desorption branch of the isotherm. The PSD peaks from both, adsorption and desorption branches, show that plasma-assisted synthesis of titania–ZF nanocomposites lead to a composite material having pores with more uniform size. Also, it can be observed that the PSD peak is narrow when the discharge time in liquid media increases. This leads to the formation of a nanocomposite with cylindrical pores having a more uniform size, as observed from the TEM images (see Fig. 3). The registered nitrogen sorption isotherms were used to calculate the BET specific surface areas (S_{BET}), total pore volumes (V_t), whereas the PSDs calculated from both adsorption and desorption branches gave the mean pore diameters (D_{pore}) (Table 1). It should be mentioned that, comparison with the ultrasound-assisted method reveals that by the plasma treatment, a mesoporous nanocomposite with a lower specific surface area can be obtained. On the other hand,

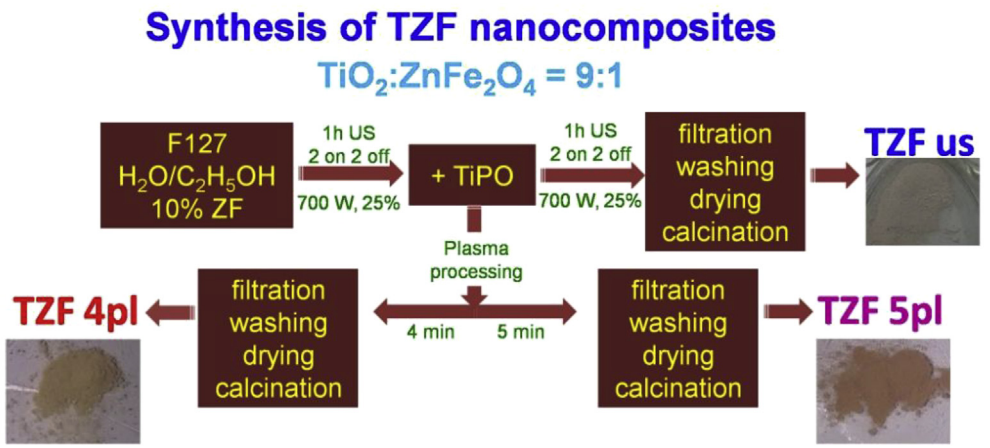

Fig. 1. Synthesis flowchart of the TZF nanocomposites by ultrasonication and plasma processing.

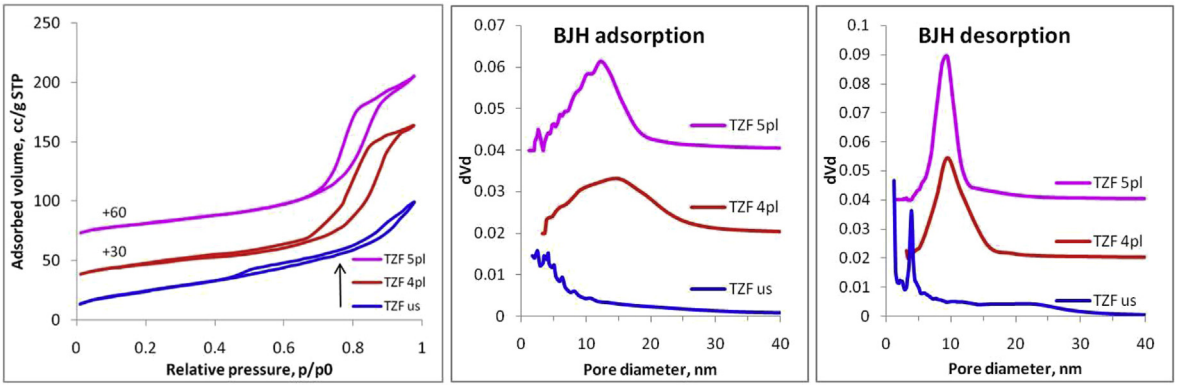

Fig. 2. Nitrogen sorption isotherms and corresponding BJH (Barett–Joyner–Halenda) pore size distributions (calculated from both adsorption and desorption branches, respectively) of nanocomposites (**TZF us**, **TZF 4pl**, and **TZF 5pl**).

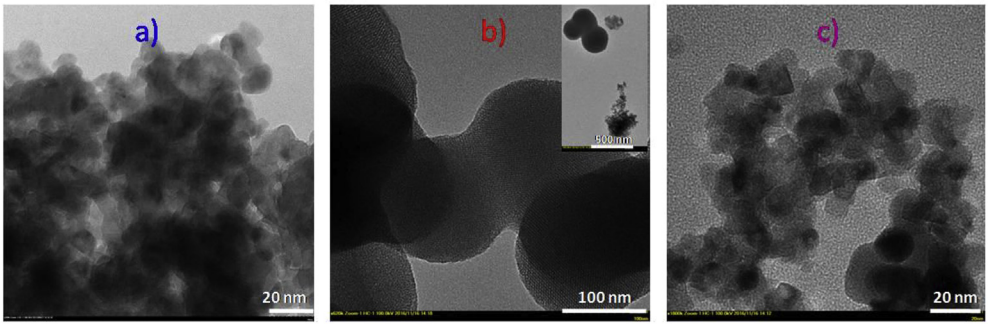

Fig. 3. Representative TEM micrographs for the titania–zinc ferrite nanocomposites: (a) **TZF us**, (b) **TZF 4pl**, and (c) **TZF 5pl**.

the total pore volume is a bit higher because of the enhancement of mesoporosity achieved by liquid plasma technique. **TZF us** sample exhibits two types of pores of different mean sizes (3.9 and 23.1 nm, respectively), whereas **TZF 4pl** and **TZF 5pl** have pores of only one size (9.3 and 9.5 nm, respectively).

The pore/particle morphology of the synthesized nanocomposites was investigated by TEM (Fig. 3). The TEM images of **TZF us** (Fig. 3a) and **TZF 5pl** (Fig. 3c) samples show homogeneous dispersed particles with a (quasi) spherical morphology. On the other hand, the TEM image of **TZF 4pl** (Fig. 3b) sample clearly shows two types of particles of different sizes: porous spherical particles associated with TiO_2 of about 200 nm and ZF (quasi)spherical particles of 10–15 nm. The titania nanoparticles show a very ordered pore network, with the pores perfectly parallel. In

Table 1
Structural, morphological, and optical features of the synthesized titania–zinc ferrite nanocomposites.

Technique		N_2-sorption				XRD	SAXS	UV–vis DR
Sample	Synthesis conditions	S_{BET}, m^2/g	$D_{pore,}$ nm (ads)	$D_{pore,}$ nm (des)	V_{pore}, cm^3/g	D_{cryst}, nm (TiO_2)	D_{SAXS}, nm	Band gap energy, eV
TZF us	Ultrasounds	92	3.9	3.9; 23.1	0.192	9.6	11.7	1.60
TZF 4pl	4 min plasma	64	15.1	9.3	0.201	9.7	5.3	1.62
TZF 5pl	5 min plasma	76	12.2	9.5	0.217	8.6	4.5	2.22

conclusion, 4 min of electrical discharge is not enough to mix the components in an intimate manner. To obtain a homogeneous nanocomposite the plasma processing must last longer.

The structural properties of the nanocomposite have been evidenced by registering the XRD patterns (Fig. 4). All these patterns show sharp peak characteristics for crystalline structures. At a closer look, one can notice the presence of crystals of both origins, as a sum of patterns, given by TiO_2 and ZF components. According to JCPDS 84-1286 card [23] the pure anatase phase of titania is found for all TZF samples. Thus, the specific (101), (004), (200), (105), and (211) XRD diffraction planes of the anatase phase are present (Fig. 4). Also, the spinel ferrite typical diffraction peaks ((220), (311), (400), (422), (511), and (440) according to JCPDS 22-1012) [24]), which are because of the presence of a pure cubic ZF structure, are clearly observed. The more intense diffraction peak, that describes the (101) diffraction plane of the crystalline anatase phase, was used to calculate the crystallite size of the titanium oxide component. As observed from Table 1, the crystallites are bigger when ultrasound treatment is used, whereas the liquid plasma processing led to smaller crystallite sizes of the TiO_2. At a longer plasma processing time, a slight increase in the crystallite size could be noted. Note that both synthesis procedures lead to the titania–ZF nanocomposite. The dissolution of titanium cations into the ferrite matrix is prevented, this fact being opposite to the reports available within the literature [7].

The SAXS profiles depicted in Fig. 5 provide information on the structural properties of the synthesized nanocomposites. The logarithmic plots of the scattered intensity

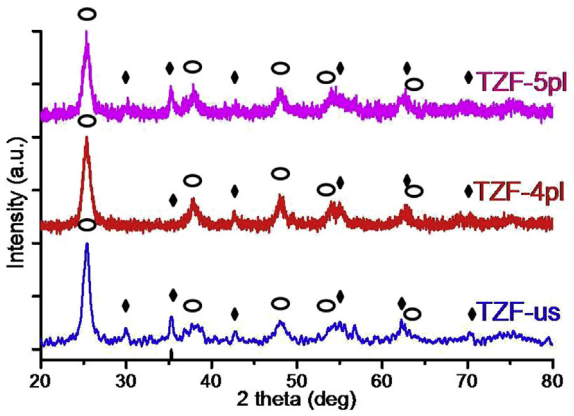

Fig. 4. XRD patterns of obtained titania–zinc ferrite nanocomposites involving ultrasounds and plasma processes (○—titania, ♦—zinc ferrite).

$I(s)$ (in arbitrary units) versus s (in inverse angstroms) show a decrease in the intensity at low angles in the series **TZF us** > **TZF 4pl** > **TZF 5pl**. The interparticle interactions are deduced from the SAXS profiles. The scattering intensity decreases for all synthesized samples indicating a repulsive behavior of the particles [25]. The attractive particle interactions seem to occur in the case of the **TZF us** nanocomposite sample that shows a steep SAXS profile with the highest intensity. Thus, the ultrasound-assisted method produces mostly aggregates of the titania–ZF nanocomposite. On the contrary, the liquid plasma processing leads to more diluted systems, slightly dispersed. This feature could be deduced from the decrease in the intensity at low s values in Fig. 5. The plasma treatment time plays an important role in the particle dispersion because the scattering intensity decreases when the processing time increases from 4 to 5 min. Furthermore, the SAXS data were used to calculate the pair distance distribution function $P(R)$. This allows the evaluation at a higher statistical level of the particle size and particle size distribution [26], being an advantage over the TEM technique. Thus, it can explain the lack of particle aggregation in dispersion, a phenomenon that is common for magnetic materials during sample preparation for TEM [26]. The $P(R)$ plots were obtained introducing collected SAXS data in ATSAS software package (GNOM) considering the size and shape polydispersity [27] and comparing the obtained curves. The resulted average particle diameters (D_{SAXS}, nm) of the synthesized TZF samples are summarized in Table 1, and the obtained values follow the same trend as the crystallite size calculated using the XRD patterns of the TiO_2 particles. As observed, the $P(R)$ function plot for the **TZF us** shows a wide peak, and the calculated average diameter for the aggregates is 11.7 nm. An important difference in the peak height and width between the TZF samples prepared by the two methods can be noticed. A decrease in the particle diameter (the peak shifts to the lower values) and a more uniform distribution (the peak narrowing is observed) for the plasma-processed TZF samples can be observed. Actually, this could be a consequence of the system dilution (low or almost no level of aggregation) where there is no spatial correlation between particles [28]. A plausible explanation for the smaller sizes of the **TZF pl** nanocomposites compared with **TZF us** sample is that the high energy released during the discharges in liquid smashes the big particles (aggregates) into smaller pieces (crystals) for longer plasma processing times.

The optical properties of the synthesized nanocomposites were studied using the Tauc plots, which allowed calculation of the corresponding indirect band gap values for the TZF nanocomposites. For this purpose, the

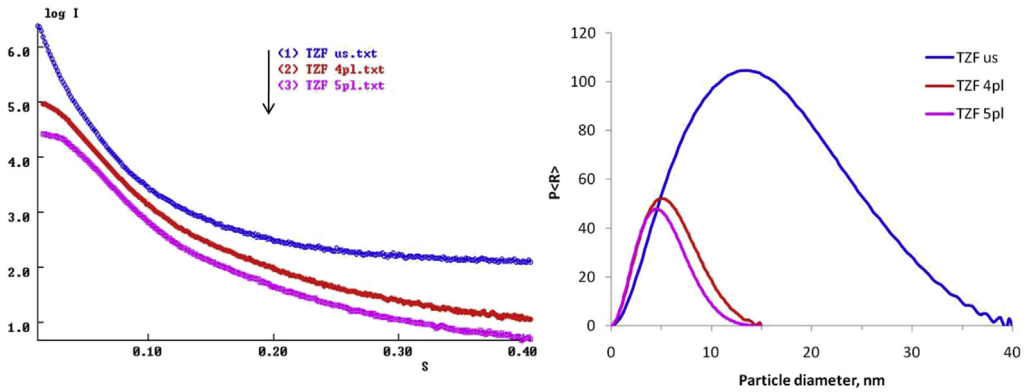

Fig. 5. (a) SAXS profiles and (b) $P(R)$ distributions for the synthesized titania–zinc ferrite nanocomposites.

Kubelka–Munk function was applied to the collected UV–vis DR spectra (Fig. 6 and Table 1). As observed, the indirect band gap values for all nanocomposites are much smaller than those of the pure titania (anatase phase—3.2 eV) [29]. This indicates that our nanocomposites are suitable to be used in the capture of the visible light and that they can be applied in photocatalysis. The lower band gap energy (1.60 eV) was found in the **TZF us** nanocomposite. This band gap value is very close to the energy value of pure ZF nanoparticles (1.40 eV) [10]. When the band gap value for the **TZF 4pl** sample was calculated, a slight increase in the energy band gap was observed (1.62 eV). This shows that both materials can be excited by light of approximately the same wavelength. The band gap widening of the previously mentioned TZF nanocomposites compared with pure ZF is explained by the synthesis technique. Thus, at the interface between titania and ZF nanoparticles an interparticle charge transfer through a natural difference in energy band level occurs, this fact being applicable to the visible light–driven photocatalysts. In contrast, the **TZF 5pl** sample has a band gap value of 2.22 eV as can be observed from the red-shift of the absorption edge, which is roughly proportional to the plasma process time. A possible explanation is related to the TiO_2 particle grinding during the plasma process so that the surface interparticle interactions between titania and ZF increase. In this case, as observed from TEM micrographs, the TiO_2 particles interact in an "intimate" manner allowing the charge transfer requested for an efficient use of sunlight in a photocatalytic process.

3.2. Photocatalytic activity

The photocatalytic activity of TZF nanocomposites was determined by the photodegradation of R6G in an aqueous solution under visible light irradiation. R6G was chosen as a probe molecule because it is not susceptible to photolysis when irradiated by visible light. Fig. 7 reveals the

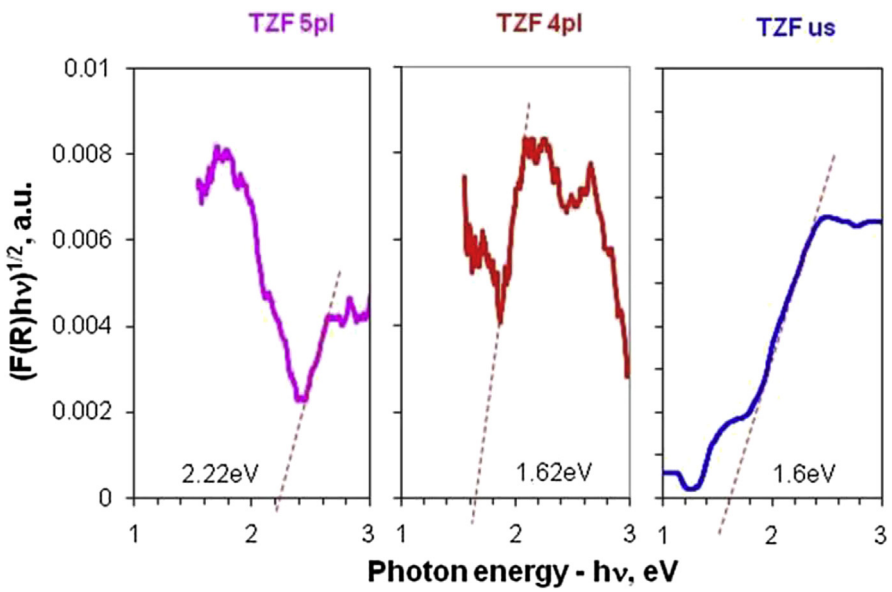

Fig. 6. Comparative Tauc plots for indirect band gaps of nanocomposites (TZF) obtained by plasma and ultrasound-assisted methods.

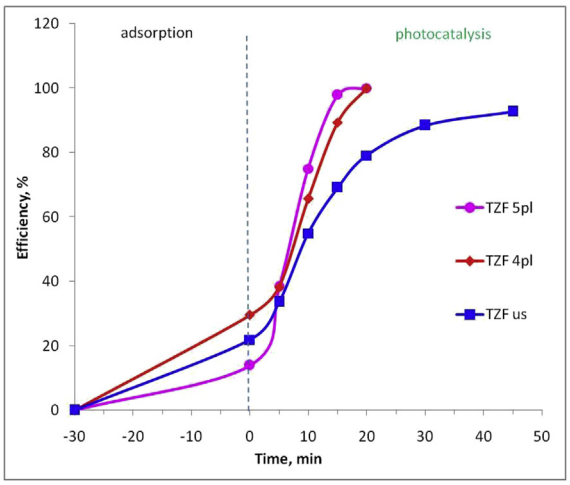

Fig. 7. Photocatalytic efficiency of the synthesized TZF nanocomposites in degradation process of Rhodamine 6G under visible light.

photocatalytic efficiency of the synthesized titania–ZF nanocomposites as a function of time. As observed, the reaction time, in the considered experimental conditions, is quite short for the plasma-synthesized samples, reaching 100% efficiency after only 20 min of the photocatalytic experiment. On the other hand, the **TZF us** nanocomposite sample shows a slower photocatalytic activity, reaching a degradation efficiency of only 93%, after 45 min of visible light irradiation. Therefore, liquid plasma processing seems to be the best for the synthesis of the TZF nanocomposite, because a photocatalyst with amazing features like average particle size, narrow band gap, high BET-specific surface area, pore size, and volume is obtained. All these features are optimal for the **TZF 5pl** sample that shows the highest photocatalytic efficiency under visible light irradiation. The photodegradation performance recommends our material as a very efficient nanophotocatalyst, compared with results previously reported concerning ZF-titania–assisted photodegradation of organic dyes [30]. One may notice that literature proposes photocatalytic efficiencies ranging from 93% to 100% after longer reaction times (60–300 min) for ZF–titania materials. Nevertheless, a proper comparison is still difficult because no data presenting exactly the same photocatalytic systems are available.

Because of its narrow band gap, the ZF is considered to act as a sensitizer [31] in TZF nanocomposites. Thus, the ZF particles are excited by photons having the wavelength within 400–450 nm range and form an electron–hole pair. Subsequently, the conduction band of TiO_2 particle is occupied by the photogenerated electron. Therefore, there are no holes in TiO_2 with which electrons may recombinate, and the electron–hole recombination is delayed. This suggests that the synthesized ZF–titania nanocomposites are expected to actively participate in reduction reactions by increasing the number of photogenerated charge carriers under visible light irradiation. In such conditions, the electrons and holes generated by the photocatalytic material can lead to the formation of O^{2-} and HO• as a result of the reaction with the surface adsorbed O_2 and H_2O [7]. The as-obtained radicals are well known as very powerful oxidative species able to transform R6G first into smaller organics and further into CO_2, H_2O, and other innocuous inorganic compounds [3].

4. Conclusions

Titanium oxide nanoparticles have been successfully produced by high-temperature liquid plasma process (such as arc discharge in liquid media) in the presence of ZF nanoparticles. The obtained nanocomposites have superior textural (porosity, pore diameter/volume), structural (anatase phase), and morphological and optical (anatase phase) properties compared with the nanocomposite synthesized by US. The pore structure depends on the synthesis method (LPP and US), as can be observed from BET measurements. In spite of a slit-like pores resulted from US, more cylindrical-like pores by applying liquid plasma were obtained. The surface area has been reduced, but the available surface increases with the exposure time to plasma. In contrast, the pore sizes are about four times larger when the plasma treatment is used and depend on the exposure time. Both considered synthesis techniques led to the formation of the anatase phase, but only the liquid plasma conduct to the formation of the titania–ZF nanocomposite particles with lower agglomeration tendency. The photocatalytic tests on R6G degradation under visible light proved the superior efficiency of the materials involving plasma treatment during synthesis.

Acknowledgments

The author P.S. is grateful for the financial support from the Romanian National Authority for Scientific Research and Innovation, CNCS—UEFISCDI, project number PN-II-RU-TE-2014-4-1266. Also, Dr. Cristian Petrica Lungu (National Institute for Laser, Plasma and Radiation Physics, Romania) is greatly acknowledged for the help and support with devices for plasma formation in liquids.

References

[1] E. Casbeer, V.K. Sharma, X.Z. Li, Sep. Purif. Technol. 87 (2012) 1.
[2] M. Abbas, B.P. Rao, V. Reddy, C.G. Kim, Ceram. Int. 40 (2014) 11177.
[3] S. Feraru, A.I. Borhan, P. Samoila, C. Mita, S. Cucu-Man, A.R. Iordan, M.N. Palamaru, J. Photochem. Photobiol. A. 307 (2015) 1.
[4] A.O. Ibhadon, P. Fitzpatrick, Catalysts 3 (2013) 189.
[5] A.I. Borhan, P. Samoila, V. Hulea, A.R. Iordan, M.N. Palamaru, J. Taiwan Inst. Chem. E. 45 (2014) 1655.
[6] N. Rezlescu, E. Rezlescu, P.D. Popa, C. Doroftei, M. Ignat, Rom. Rep. Phys. 65 (4) (2013) 1348.
[7] K. Natarajan, P. Singh, H.C. Bajaj, R.J. Tayade, Korean J. Chem. Eng. 32 (4) (2015) 1.
[8] A. Šutka, M. Millers, N. Döbelin, R. Pärna, M. Vanags, M. Maiorov, J. Kleperis, T. Käämbre, U. Joost, E. Nõmmiste, V. Kisand, M. Knite, Phys. Status Solidi A 212 (4) (2015) 796.
[9] Y. Yao, J. Qin, H. Chen, F. Wei, X. Liu, J. Wang, S. Wang, J. Hazard. Mater. 291 (2015) 28.
[10] M. Ignat, R. Rotaru, P. Samoila, L. Sacarescu, D. Timpu, V. Harabagiu, C. R. Chimie (2016), http://dx.doi.org/10.1016/j.crci.2016.11.004.
[11] J. Zheng, R. Yang, L. Xie, J. Qu, Y. Liu, X. Li, Adv. Mater. 22 (13) (2010) 1451–1473.
[12] T.A. Kareem, A.A. Kaliani, Ionics 18 (3) (2012) 315–327.
[13] G. Saito, T. Akiyama, (2015) http://dx.doi.org/10.1155/2015/123696.
[14] N. Saito, J. Hieda, C. Miron, O. Takai, J. Surf. Finish. Soc. Jpn. 58 (2007) 112.
[15] Y. Ichino, K. Mitamura, N. Saito, O. Takai, J. Vac. Sci. Technol. A. 27 (2009) 826.

[16] O. Takai, Pure Appl. Chem. 80 (9) (2008) 2003–2011.
[17] P. Samoila, C. Cojocaru, I. Cretescu, C.D. Stan, V. Nica, L. Sacarescu, V. Harabagiu, J. Nanomater. (2015), http://dx.doi.org/10.1155/2015/713802, ID 713802.
[18] C.P. Lungu, A.M. Lungu, P. Chiru, O. Pompilian, N. Georgescu, M. Magureanu, I. Mustata, T. Velea, D. Stanciu, V. Predica, Rom. J. Phys. 54 (2009) 369.
[19] C. Miron, I. Sava, I. Jepu, P. Osiceanu, C.P. Lungu, L. Sacarescu, V. Harabagiu, Plasma Proc. Polym. 10 (2013) 798.
[20] C. Coromelci-Pastravanu, M. Ignat, E. Popovici, V. Harabagiu, J. Hazard. Mater. 278 (2014) 382.
[21] M. Thommes, K.A. Cychosz, Adsorption 20 (2014) 233.
[22] M. Thommes, K. Kaneko, A.V. Neimark, J.P. Olivier, F. Rodriguez-Reinoso, J. Rouquerol, K.S.W. Sing, Pure Appl. Chem. 87 (2015) 1051, http://dx.doi.org/10.1515/pac-2014-1117.
[23] S.M. El-Sheikh, T.M. Khedr, A. Hakki, A.A. Ismail, W.A. Badawy, D.W. Bahnemann, Sep. Purif. Technol. 173 (2017) 258.
[24] A.N. Birgani, M. Niyaifar, A. Hasanpour, J. Magn, Magn. Mater. 374 (2015) 179.
[25] C.R. Mosbaek, P.V. Konarev, D.I. Svergun, C. Rischel, B. Vestergaard, Pharm. Res. 29 (2012) 2225–2235.
[26] V. Goertz, N. Dingenouts, H. Nirschl, Part. Part. Syst. Charact. 26 (2009) 17.
[27] M.V. Petoukhov, D. Franke, A.V. Shkumatov, G. Tria, A.G. Kikhney, M. Gajda, C. Gorba, H.D.T. Mertens, P.V. Konarev, D.I. Svergun, J. Appl. Cryst. 45 (2012) 342.
[28] A. Gunier, G. Fournet, Small Angle Scattering of X-rays, John Wiley, 1955.
[29] T. Luttrell, S. Halpegamage, J. Tao, A. Kramer, E. Sutter, M. Batzill, Sci. Rep. 4 (4043) (2014) 1.
[30] J. Gómez-Pastora, S. Dominguez, E. Bringas, M.J. Rivero, I. Ortiz, D.D. Dionysiou, Chem. Eng. J. 310 (2017) 407.
[31] K.R. Gopidas, M. Bohorquez, P.V. Kamat, J. Phys. Chem. 94 (16) (1990) 6435–6440.